JOURNAL OF GEOPHYSICAL RESEARCH VOL. 74, NO. 27, DECEMBER 15, 1969

Diffuse Component of Lunar Radar Echoes

ALAN A. BURNS

Radio Physics Laboratory, Stanford Research Institute
Menlo Park, California 94025

A simple model consisting of volume backscattering from within the lunar regolith can explain the observed diffuse component of lunar radar echoes. At a wavelength of 68 cm, a good match of the model with the data yields a value of 2.5–3 for the relative permittivity of the regolith in good agreement with the quasi-specular backscattering estimates. The fit at 23 cm is poorer but yields a value slightly less than 2. At 3.8 cm, the value is below 1.5, and both that value and the 23 cm value are in good agreement with the radiometrically determined values at their respective wavelengths. These lower values at short wavelengths are probably a result of the rapid density increase with depth just at the surface. A slope-dependent reflectivity can reconcile the values of relative permittivity obtained radiometrically and from the proposed diffuse backscattering model to those obtained from radar cross-section measurements. There is some evidence that the permittivity of the rocks forming the lunar highlands may be lower than that of the rocks underlying the maria.

In a recent paper, the author [*Burns*, 1969] proposed that the diffuse component of lunar radar echoes primarily arose from volume backscattering from within the surface layer, or regolith. This model resulted from the observation of very near wavelength independence of the diffuse component over a very wide interval (at least 23 cm–7.5 m) and the inadequate number of visible small-scale surface features to account for the observed echo strength (see Appendix 1). In particular, as a preliminary finding, the hitherto unexplained $\approx \cos^{3/2} \theta$ dependence of the diffuse component for $0.7 < \cos \theta < 0.2$, where θ is the angle of incidence on the surface, was stated to be a result of this type of scattering.

According to our model, the division of lunar radar echoes into diffuse and quasi-specular components is thus primarily a division into scattering from within the regolith and reflection from its surface, except where the regolith is optically thin and reflections from the subregolithic surface become important [*Burns*, 1969]. Although several authors have attributed lunar backscatter at all angles of incidence to quasi-specular or purely geometric optics reflections and have been successful in matching the observed backscattering behavior with various surface models [*Muhleman*, 1964; *Beckmann*, 1965], we believe, in agreement with *Evans and Hagfors* [1966], that the diffuse component is actually due to small-scale features. In order to explain their observational results at 23 cm, *Hagfors et al.* [1965] proposed that the small-scale features were buried beneath a tenuous layer greater than 20 cm deep. Later, however, the visible objects on the surface were thought to be responsible for the diffuse component [*Hagfors*, 1967; *Lincoln Laboratory*, 1967]. A numerical error, however, led to a 20 db overestimate of the scattered power (Appendix 1); hence the explanation of *Evans and Hagfors* [1966] appears to be the correct one. Our volume backscattering model represents an extension of that explanation. A major difficulty with attributing the diffuse component to small-scale elements was the lack of an adequate explanation for the observed $\approx \cos^{3/2} \theta$ angular power law at high incidence angles. Scattering from within the regolith, a translucent medium to radio waves, seems to supply that explanation, as well as accounting for the polarization results.

Our fundamental diffuse backscattering model is quite simple. It merely consists of a plane surface (the effects of roughness will be considered below) separating half-spaces of vacuum and a medium of relative permittivity ϵ_r. The angles of incidence and transmission are θ and ϕ respectively. Within the regolith there are irregularities, perhaps dense rocks and

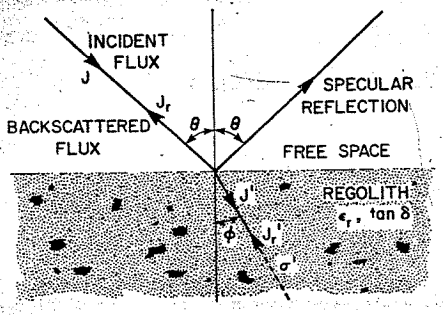

Fig. 1. Diffuse backscattering model.

boulders such as those photographed on the lunar surface, that present a certain backscattering 'cross section' per unit projected area σ' (this quantity will be defined precisely below) to an incident wave in the regolith (Figure 1). As noted in the previous article [*Burns*, 1969], the scattering volume is limited in depth by attenuation due to losses in the regolith and is therefore strongly wavelength dependent. (For a constant loss tangent, the scattering volume will be proportional to the wavelength.) This implies that the regolith must be quite deep in general to avoid limiting of the scattering volume by the subregolithic surface, although such a limitation may be the reason highland areas are better backscatterers than maria (see Appendix 3).

We shall ignore multiple reflections from the small-scale objects and from the surface itself. The primed quantities apply within the regolith, and the cross sections will always be either per unit surface or per projected area. We shall not be concerned here with the precise nature of the objects and their scattering behavior. In our previous article [*Burns*, 1969], however, we noted that their cumulative size distribution, assuming that their cross section is proportional to their physical size, should have an inverse third power dependency if the diffuse component is to be strictly wavelength independent. This is exactly the law predicted for rubble due to meteoroid bombardment [*Shoemaker et al.*, 1968]. The magnitude of backscattered power predicted by this model also appears consistent with the observed levels. These points are discussed in Appendix 2.

Let S be the incident flux density above the surface. Then $J = S \cos\theta$ is the incident power per unit surface area. The radar cross section is proportional to

$$\sigma = \frac{\text{backscattered flux per unit surface area}}{\text{incident flux density}}$$

$$\sigma = (J_r/S) = (J_r/J)\cos\theta$$

where J_r is the transmitted backscattered flux per unit surface area. Let T and T' be the transmissivities given by $T = J'/J$ and $T' = J_r/J_r'$ where the relation $J_r' = \sigma' J'$ defines σ'. Then $\sigma = TT'\cos\theta\,\sigma'$. T and T' are obtained from the 'Fresnel formulae' [*Born and Wolf*, 1965]. We shall assume that σ' is independent of θ.

First, suppose that there is no depolarization below the surface. For an incident wave linearly polarized in the plane of incidence,

$$\sigma_\parallel = T_\parallel T_\parallel' \cos\theta\sigma_s'$$

where the s subscript denotes 'specular' reflection; for polarization perpendicular to the plane of incidence,

$$\sigma_\perp = T_\perp T_\perp' \cos\theta\phi_s'$$

The products are

$$F_\perp = T_\perp T_\perp' = \frac{16\sin^2\phi\cos^2\phi\sin^2\theta\cos^2\theta}{\sin^4(\phi+\theta)}$$

$$F_\parallel = T_\parallel T_\parallel' = F_\perp\cos^{-4}(\phi-\theta)$$

$$F_g = T_\perp T_\parallel' = T_\parallel T_\perp' = F_\perp\cos^{-2}(\phi-\theta)$$

Snell's law relates the angles:

$$\sin\theta = (\epsilon_r)^{1/2}\sin\phi$$

Even if there were no depolarization below the surface, there is in general some depolarization of a linearly polarized incident wave with angle ζ between incident and polarization planes. This is due to a rotation of the polarization plane by the surface. The expected component is

$$\sigma_{El_s} = (F_\parallel\cos^4\zeta + F_\perp\sin^4\zeta + 2F_g\sin^2\zeta\cos^2\zeta)\cos\theta\sigma_s'$$

where F_g is the geometric mean of $F_\parallel$ and $F_\perp$, and the depolarized component is

$$\sigma_{Dl_s} = 2(F_a - F_g)\sin^2\zeta\cos^2\zeta\cos\theta\sigma_s'$$

where F_a is the arithmetic mean of $F_\parallel$ and $F_\perp$. Averaged over all ζ these become

$$\bar\sigma_{El_s} = \tfrac{1}{4}(3F_a + F_g)\cos\theta\sigma_s'$$

and

$$\bar\sigma_{Dl_s} = \tfrac{1}{4}(F_a - F_g)\cos\theta\sigma_s'$$

Now suppose that there is a component of σ', σ_d', that specifies the amount of the incident wave converted into the orthogonal linear polarization. In this case, the rotations of the polarization planes at the surface are opposite for the incident and reflected waves; hence there is no coupling back into the expected component for the surface, and the cross section is independent of ζ. Therefore

$$\bar\sigma_{Dl_d} = \sigma_{Dl_d} = F_g\cos\theta\sigma_d'$$

Since the powers add, the cross sections from the two sources are just $\bar\sigma_{El} = \bar\sigma_{El_s}$ and $\bar\sigma_{Dl} = \bar\sigma_{Dl_s} + \sigma_{Dl_d}$.

It is convenient now to introduce a simple model for the backscattering with the regolith for comparing linear with circular polarization. Following *Evans and Hagfors* [1966] and *Hagfors* [1967], let us suppose that this backscattering is described by a collection of randomly oriented 'dipoles' and nondepolarizing 'facets' of total cross sections σ_{dp}' and σ_f' respectively. Then for linear incident polarization, assuming that the contributions from 'dipoles' and 'facets' add incoherently (it actually makes no difference whether the 'dipoles' and 'facets' add incoherently or not, for any contribution due to coherence simply increases the apparent value of σ_f'), we have $\sigma_r' = \sigma_f' + \tfrac{3}{4}\sigma_{dp}'$, and $\sigma_d' = \tfrac{1}{4}\sigma_{dp}'$.

Thus

$$\bar\sigma_{El} = \tfrac{1}{4}[(3F_a + F_g)(\sigma_f' + \tfrac{3}{4}\sigma_{dp}')]\cos\theta$$

and

$$\bar\sigma_{Dl} = \tfrac{1}{4}[(F_a - F_g)\sigma_f' + (3F_a + F_g)\tfrac{1}{4}\sigma_{dp}']\cos\theta$$

Consider now circular incident polarization. Both the 'dipoles' and the 'facets' contribute to the expected and the depolarized echo components. In the 'dipole' case, there is equal contribution; the cross sections are

$$\sigma_{Ecd} = \sigma_{Dcd} = \tfrac{1}{8}(3F_a + F_g)\cos\theta\sigma_{dp}'$$

which have the same shape as $\bar\sigma_{El_s}$. For the 'facets,' the cross sections are

$$\sigma_{Ecf} = \tfrac{1}{2}(F_a + F_g)\sigma_f'\cos\theta$$

and

$$\sigma_{Dcf} = \tfrac{1}{2}(F_a - F_g)\sigma_f'\cos\theta$$

Combining both mechanisms,

$$\sigma_{Ec} = \tfrac{1}{2}[\tfrac{1}{4}(3F_a + F_g)\sigma_{dp}' + (F_a + F_g)\sigma_f']\cos\theta$$

and

$$\sigma_{Dc} = \tfrac{1}{2}[\tfrac{1}{4}(3F_a + F_g)\sigma_{dp}' + (F_a - F_g)\sigma_f']\cos\theta$$

These expressions are very similar to those for linear incident polarization; the latter is just twice the corresponding expression for linear depolarization.

To give some feeling for the natures of the various quantities involved, $F_\perp\cos\theta$ and $F_\parallel\cos\theta$ are plotted in Figure 2 for several values

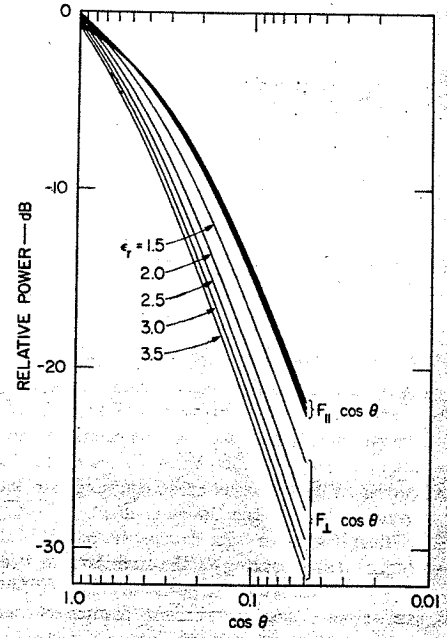

Fig. 2. Relative permittivity dependence of the basic cross-section quantities.

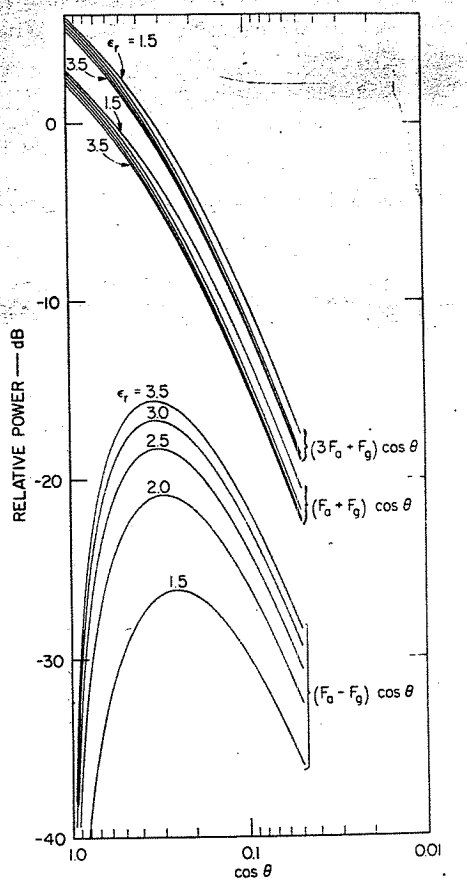

Fig. 3. Relative permittivity dependence of the functions forming the expressions for the cross sections.

of ϵ_r. Similarly, $(3F_a + F_g)\cos\theta$, $(F_a + F_g)\cos\theta$, and $(F_a - F_g)\cos\theta$ appear in Figure 3. It is clear that all but $(F_a - F_g)\cos\theta$ are generally very close to a $\cos^{3/2}\theta$ law over a wide range of $\cos\theta$. Of the others, $F_\parallel \cos\theta$ has the poorest fit owing to enhanced coupling into the surface related to the Brewster effect.

Thus, whatever the nature of σ', if it is nearly independent of θ (the simplest and perhaps a not unreasonable possibility), this model can explain the most salient feature of the observed diffuse behavior. Except for the depolarized circular echoes, which very closely follow a $\cos\theta$ law [*Evans and Pettengill*, 1963], the various other diffuse echo components have a $\approx\cos^{3/2}\theta$ dependence for $0.7 \geq \cos\theta \geq 0.2$. The circular expected echoes for $\lambda \geq 23$ cm seem to follow $\cos^{3/2}\theta$ rather closely, but at $\lambda = 23$ cm, which is the shortest wavelength at which the linear polarization diffuse component has been observed [*Hagfors*, 1967], both the expected and depolarized lunar components appear to have somewhat smaller exponents than 3/2. (Although we shall often use the $\cos^{3/2}\theta$ law to represent the experimental results here, we do not feel that it, in fact, truly represents the backscattering law.) For $\cos\theta \leq 0.1$–0.2, the echoes tend to follow a $\cos\theta$ law, which is possibly explained by including surface rocks (Appendix 1) and roughness in the present model.

Before considering the effects of roughness, let us attempt to fit the facets-plus-dipoles-within-the-regolith model to the data. There are two independent quantities: the relative permittivity and the ratio of total 'dipole' cross section to 'facet' cross section. Since the two quantities have different functional dependencies, they can be separately estimated fairly well. By noting any differences between the circular and linear polarization results, one can check the model for consistency. Only at 23 cm is there a complete series of measurements with circular and linear polarization; at that wavelength the rapid increase in regolithic density in the first few centimeters below the surface [*Jaffe*, 1968; *Jones*, 1968] should become very important to the reflectivity and transmissivity. The former effect reduces the surface reflectivity, and therefore the apparent permittivity, and may possibly introduce a considerable degree of incidence angle sensitivity [*Lincoln Laboratory*, 1966].

Figures 4 and 5 show the angular variation of $\bar{\sigma}_{El}$, $\bar{\sigma}_{Dl}$ and σ_{Ec}, σ_{Dc} normalized to $\sigma_T' = \sigma_{dp}' + \sigma_f'$ for $\epsilon_r = 2$ and 3 as parametric functions of $r = (\sigma_{dp}'/\sigma_f')$. Similarly, Figure 6 shows the ratios of these quantities over a wider range of relative permittivities. At the smaller incidence angles both the expected and depolarized components tend toward a $\cos\theta$ dependence, with the depolarized components maintaining it longer. Eventually all the components acquire a $\approx\cos^{5/2}\theta$ dependence at oblique incidence according to our model, but since roughness should be most important there, we cannot expect a fit with the observational data. Because the behavior of the expected components for $\cos\theta > 0.7$ is obscured by the quasi-specular peak, the predicted $\cos\theta$ dependence of the diffuse expected components near normal incidence cannot be seen.

Matching the model to the data is best done with the ratios. This is shown in Figure 7 for the 68-cm data [*Evans and Pettengill*, 1963]. A value of ϵ_r between 2.5 and 3.0, and of r somewhat above 0.5, gives a good fit beyond the influence of the quasi-specular peak. The fit for the 23-cm data [*Hagfors*, 1967] is not very good, particularly for circular polarization (Figure 7*b*), and is apparently due to quasi-specular peak. At high angles of incidence, however, values of ϵ_r and r somewhat less than 2 and 0.7, respectively, provide the best fit. These values are consistent between circular and linear polarization. There are two other 23-cm radar polarization measurements [*Hagfors*, 1967] with which to match the model. These appear in Figure 8 and are consistent with the other fits. Also in Figure 8(*b*) are the 3.8-cm results [*Hagfors*, 1967] indicating an even smaller value for ϵ_r, less than 1.5. Figure 9 compares the 68-cm data to the model with $\epsilon_r = 2.5$ and $r = 0.5$. The parameter r depends on the scattering behavior of the buried objects; its significance is beyond the scope of this paper.

Both these 3.8- and 23-cm values of ϵ_r are slightly smaller than the ones determined radiometrically at those wavelengths (2.1 at $\lambda = 21$ cm [*Heiles and Drake*, 1963]; 1.7–1.8 at 3.8 cm [*Lincoln Laboratory*, 1966]) although the agreement is quite good. It should be noted that the radiometric measurements refer to the entire lunar surface, but that the diffuse backscattering comes primarily from those parts

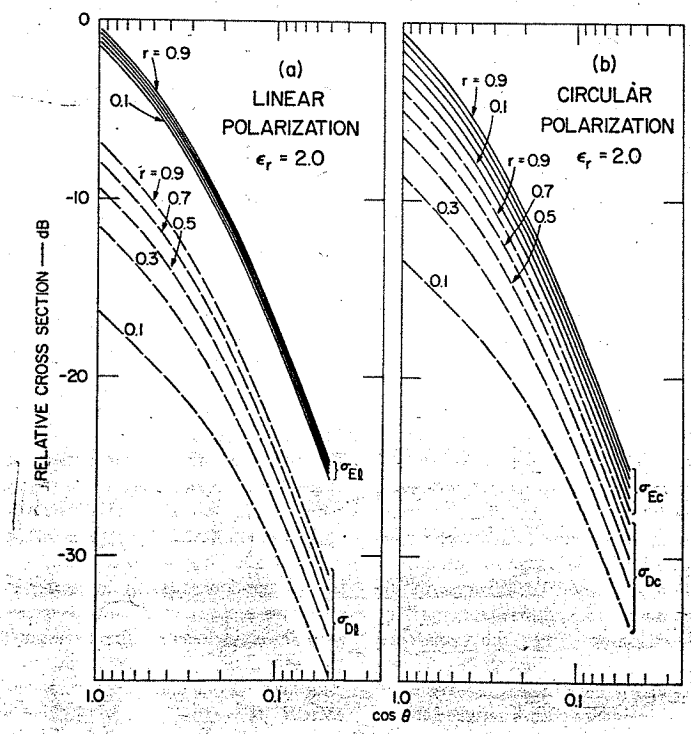

Fig. 4. Predicted diffuse cross sections for $\epsilon_r = 2.0$; r is the fraction of subsurface cross section contributed by 'dipoles.'

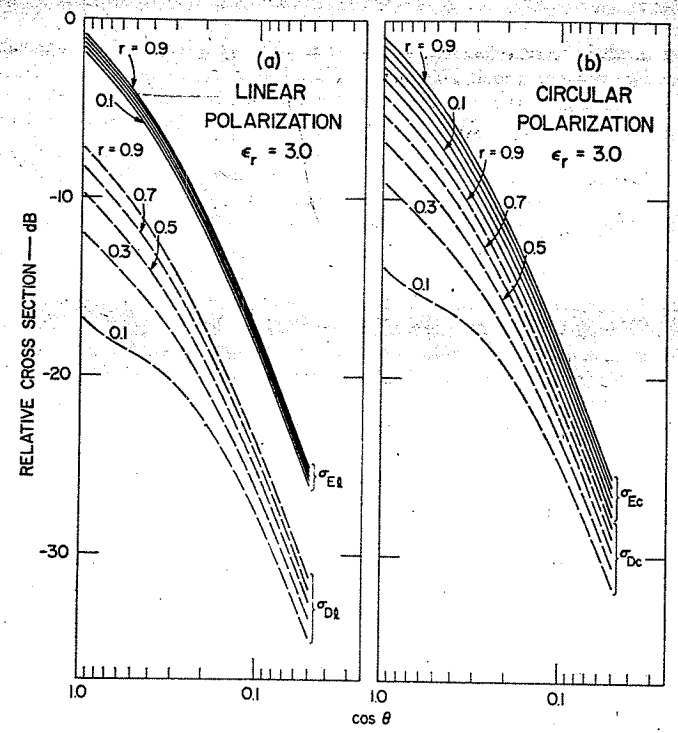

Fig. 5. Predicted diffuse cross sections for $\epsilon_r = 3.0$.

where there is a fairly deep regolith; the bare rock surfaces do not contribute appreciably to diffuse backscatter in our model since there would not likely be any suitable irregularities below those surfaces. Thus one would expect a higher value for radiometrically determined ϵ_r than for that following from our proposed diffuse backscattering model.

Measurements of the quasi-specular component at a 2-meter wavelength over a wide area show that most of the lunar surface has an rms slope considerably less than 0.1 rad (Tyler, private communication). The author obtained a unidirectional rms slope of 0.073 rad in the 6- to 12-meter range in a rough area just south of Sinus Medii and showed that the slopes are nearly normally distributed [*Burns*, 1969]. For an incidence angle θ and angle ζ between the polarization and incidence planes referred to the mean surface, the corresponding quantities, γ and ξ, for a surface element whose normal makes polar and azimuthal angles α and β, are obtained from

$$\cos\gamma = \cos\theta\cos\alpha + \sin\theta\sin\alpha\cos\beta$$

and

$$\sin(\zeta - \xi) = \sin\alpha\frac{\sin\beta}{\sin\gamma}$$

Whereas the effect of roughness on incidence angle thus becomes more important when θ becomes large, the effect on polarization has the opposite behavior, being greatest at low incidence angles. Besides the 'smearing out' effect in incident polarization and angle, roughness also causes shadowing that becomes important at oblique incidence. The necessary averaging to determine the mean cross sections when roughness is included becomes very complicated.

The general features of the roughness effects can be anticipated without actually performing the averaging. In the case of circular depolarization, the orientation of the local normal is important only in determining the incidence angle. Similarly, for linear incident polarization, averaging over all orientations of the polarization plane to the mean surface tends to eliminate the effect of roughness with respect to polarization. This will not be true when only a part of a range ring is studied with a fixed orientation of either linear incident or reflected polarization. For an entire range ring, the 'polarization smearing' will not be an important effect, particularly for the small values of rms slope apparently characterizing the regolithic lunar surface. Most importantly, the nearly identical behavior of all the components at high incidence angles indicates that roughness, while strongly affecting the cross sections themselves at high incidence angles, apparently has only a slight effect on their ratios; this is particularly true for a Gaussian-slope distribution with a small value of rms slope [*Hagfors and Morriello*, 1965]. Thus the curves of Figures 6 and 7 should be fairly accurate even in the presence of roughness, and the conclusions drawn from them should be valid. Roughness may have a greater effect on the curves of Figure 8, particularly in (*b*), where the curves lie below what would actually be obtained for any given value of ϵ_r. Finally, roughness will tend to raise the curves of Figures 4 and 5 as $\cos\theta \to 0$, for the surface elements tilted towards the observer will contribute more to the backscattered power than will be removed by elements tilted away.

The value of ϵ_r(2.5–3.0) at 68 cm obtained from our model is in good agreement with that

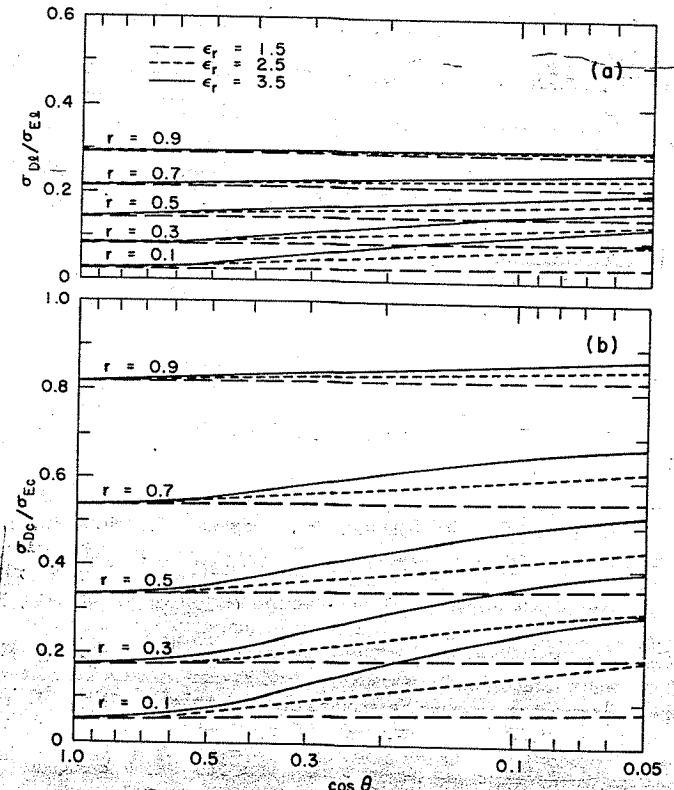

Fig. 6. Ratios of predicted diffuse cross sections: (a) linear polarization; (b) circular polarization.

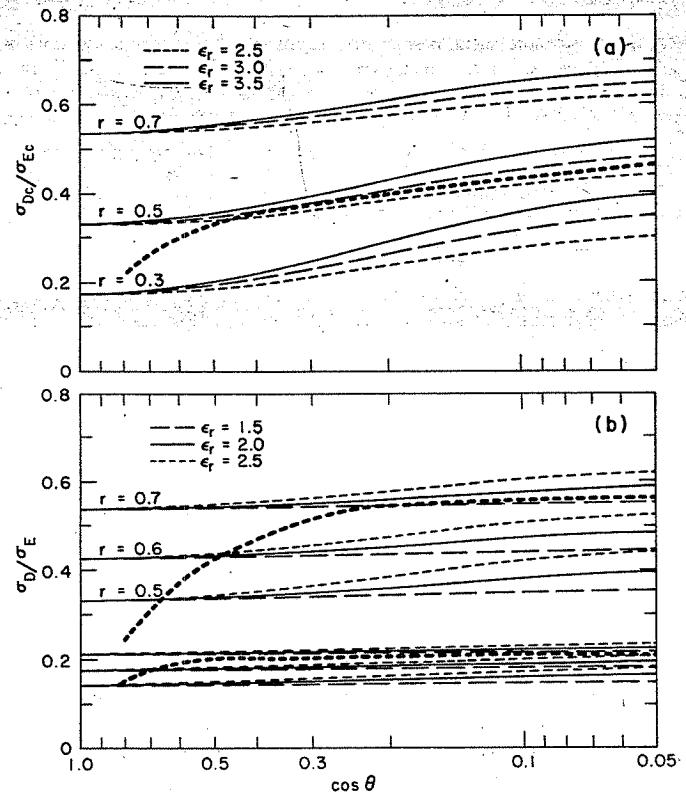

Fig. 7. Comparison of predicted cross-section ratios to observations: (a) 68-cm circular polarization; (b) 23-cm linear and circular polarizations (the upper set are the circulars).

deduced for the lunar surface from measurements of the total cross section [*Rea et al.*, 1964; *Evans and Hagfors*, 1966]. That latter value, between 2.6 and 2.8, is somewhat less than the one (3.0 ± 0.2) obtained from the most direct measurement, that of the Brewster angle by *Tyler* [1968] at a wavelength of 2.2 meters. This leads us to believe that the 68-cm value of regolithic ϵ_r is only slightly affected by the finite-distance transition at the surface. The 3.8- and 23-cm values are certainly strongly affected. But at these latter wavelengths, the relative permittivity obtained from average quasi-specular reflectivity is only slightly lower than that at 68 cm, as are, apparently, the total radar cross sections of the moon.

The inconsistent values of the relative permittivities obtained using different methods at 23 cm must be resolved. In our previous article we argued that the surface elements contributing to the quasi-specular component at incidence angles to the mean surface greater than 10° or so were bare rock surfaces, or at least surfaces with a very thin covering layer. Although very little of the total quasi-specular power comes from these elements, they are very important in determining the average reflectivity, as can be seen from the following formula of *Rea et al.* [1964]:

$$\langle R \rangle_b = \tfrac{1}{2} F(0) \int_0^{2\pi} P(\theta) \sin\theta \, d\theta$$

where

$\langle R \rangle_b$ = average backscattering reflectivity

$F(0)$ = reflectivity at normal incidence

$P(\theta)$ = normalized quasi-specular angular power law

The contribution of echoes from the regolithic surface is mainly confined to very low incidence angles but is given little weight in the integral above due to the sin θ factor. Thus a low value of regolithic reflectivity would be consistent with the observed behavior if our quasi-specular backscattering model is correct.

Further, following this model, one finds evidence that the reflectivity at normal incidence at 23 cm is lower than that at 68 cm. If we normalize the angular spectra at those two wavelengths to one other in the region beyond 10°, where the reflectivities of the bare rock surfaces should be nearly wavelength independent, we obtain the curves shown in Figure 10. The distribution of slopes is so nearly the same in both cases that the 2-db drop in the 23-cm curve at very low incidence angles must be due to a reduction in reflectivity rather than to an increase in roughness. A slight decrease in total cross section would then be observed since this normalization also effectively removes the wavelength dependence of the diffuse component. The nominal value of the measured cross section is indeed slightly lower at 23 cm than at 73 cm [*Evans and Hagfors*, 1966]. That difference is not statistically significant, however. Supposing that an apparent value for the regolithic ϵ_r of 2.6 characterizes the 68-cm low incidence angle results, the 2-db drop at 23 cm leads to an apparent value of $\epsilon_r = 2.1$ there.

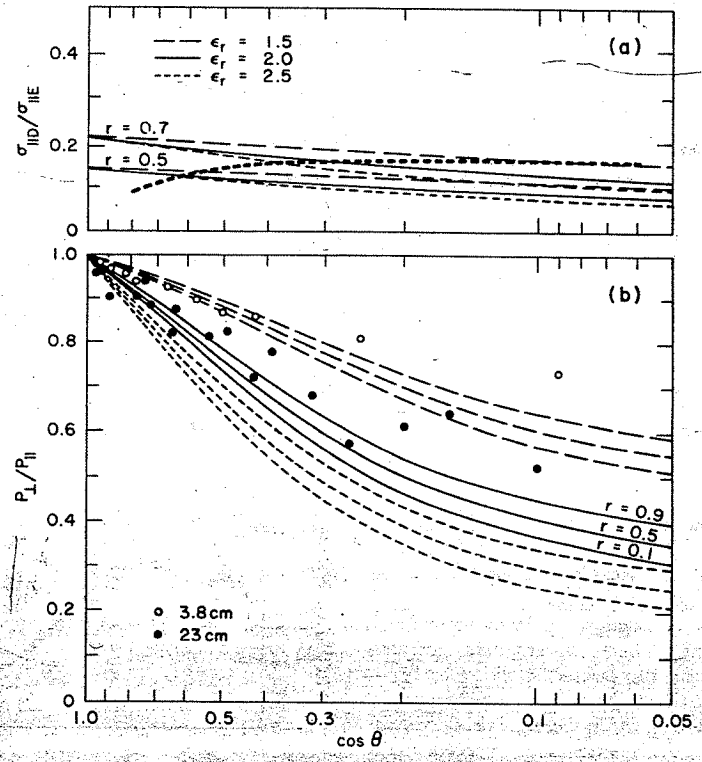

Fig. 8. Comparison of 3.8- and 23-cm data to model: (a) the ratio of depolarized to expected linear power when the incident wave is linearly polarized in the plane of incidence; (b) the ratio of echo power linearly polarized perpendicular to the plane of incidence to that in the plane of incidence for circularly polarized illumination.

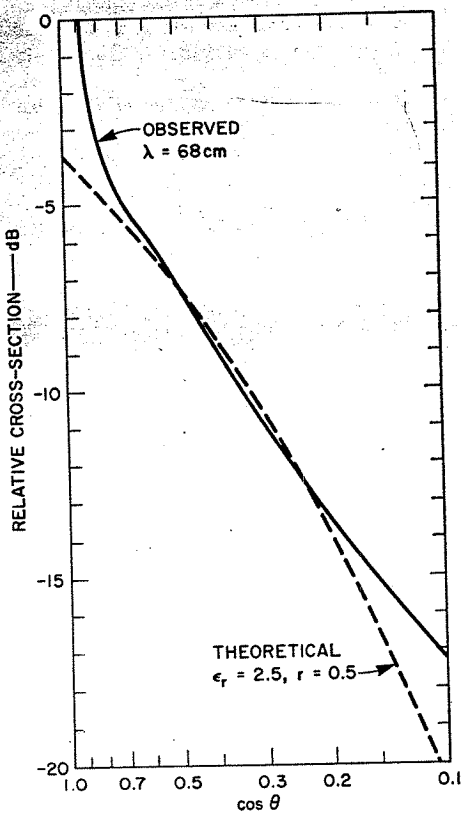

Fig. 9. Comparison between the 68-cm data and diffuse backscattering model. Vertical positions of the curves have been adjusted for a close match.

This value agrees well with the slightly lower ones deduced above and is the same as that obtained from the radiometric observations at $\lambda = 21$ cm [*Heiles and Drake*, 1963]. Thus it appears that the proposed quasi-specular backscattering model is successful in reconciling the values of ϵ_r obtained by different methods.

Presumably the bare, or nearly bare, rock surfaces are primarily located in the older highland regions. That the values for relative permittivity at 68 cm for the regolith alone and for the surface as a whole are not very different indicates that ϵ_r for these bare surfaces may not be much greater than that of the regolith itself. Figure 11 shows the results of a crude division of the quasi-specular echo into regolithic and bare-rock components. All the power for incidence angles below 10° is assigned to the regolithic surface, and all for angles above 10° is assigned to the bare rock surfaces. A numerical integration following *Rea et al.* [1964] is performed. Although the separation is admittedly crude, the general features should be correct.

In order for there to be a relatively large change in the apparent value of ϵ_{r1} (say from 2.1 at 23 cm to 2.6 at 68 cm) with only a small change in total cross section, the value of ϵ_{r2} cannot be as great as that estimated for the mare sub-regolith. (That estimate was 13 but had rather large estimated errors, leading to a lower value of 9 [*Burns*, 1969]).

The large possible errors in the measurements of the total cross section make this conclusion very speculative. Although the nominal values of the measurements indicate a relatively small change in cross section and therefore a low value of ϵ_{r2}, and although some authors treat the cross section as being wavelength independent [*Hagfors*, 1967], final resolution of this question will have to await more precise measurements of lunar scattering properties.

Appendix 1

Hagfors [1967] discussed the approximate magnitude of backscattered power from rocks seen in Surveyor 1 pictures. His model assumed that each object backscatters with a constant fraction of the geometric cross section if the diameter exceeded the wavelength and is zero

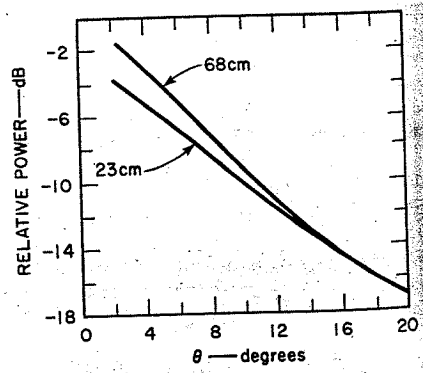

Fig. 10. The 23- and 68-cm echo power at small angles of incidence.

otherwise. In *Lincoln Laboratory* [1967] this model was applied (unfortunately, a numerical error led to a 20 db overestimate of the cross section there) to the revised Surveyor 1 and to the Surveyor 3 cumulative rock distributions. These are [*Shoemaker et al.*, 1968]:

$$\text{Surveyor 1:} \quad N_{S1} = 5 \cdot 10^5 y^{-2.2}$$

$$\text{Surveyor 3:} \quad N_{S3} = 3 \cdot 10^6 y^{-2.56}$$

where N = cumulative number per 100 m² and y is the diameter in millimeters. To these we add the Luna 9 distribution [*Smith*, 1967]

$$N_{L9} = 2 \cdot 10^6 y^{-2.9}$$

and the Surveyors 5 and 6 distributions

$$N_{S5} = 1 \cdot 10^6 y^{-2.6} \qquad \text{[Shoemaker et al., 1967]}$$

$$N_{S6} = 5 \cdot 10^6 y^{-2.5} \qquad \text{[Morris et al., 1968]}$$

Writing the cumulative distribution as $N = N_0 y^{-m}$, we then obtain for the cross section per unit area $\sigma = Ck\lambda^{-(m-2)} \cos\theta$ where k is the reflectivity of the objects and $C = (\pi/4)N_0(m/m-2)$. The following table gives the values of C and m for the various distributions:

	C_1	$m-2$
$S1$	$1.1 \cdot 10^{-2}$	0.2
$S3$	$2.2 \cdot 10^{-3}$	0.56
$S5$	$5.4 \cdot 10^{-4}$	0.6
$S6$	$6.2 \cdot 10^{-4}$	0.5
$L9$	$1.0 \cdot 10^{-4}$	0.9

where λ is in meters. Supposing k to correspond to the value for large dielectric spheres with $\epsilon_r = 9$, $k = 0.25$, we obtain the following values for cross section per unit area expressed in db:

λ, cm	σ_{S1}	σ_{S3}	σ_{S5}	σ_{S6}	σ_{L9}	Observed
3.8	−22.7	−24.5	−30.3	−31.9	−33.2	−13.6
23	−24.3	−27.9	−34.9	−34.9	−40.3	−16.3
68	−25.2	−31.5	−37.7	−37.3	−44.2	−16.9

The observed values are the diffuse components (data from *Hagfors* [1967] but with the 68-cm value renormalized to a 7.4% total cross section) extrapolated from the $0.7 > \cos\theta > 0.2$ interval to $\theta = 0$. Thus if the model for the radar cross section of each object is reasonably accurate and these distributions are typical of most of the lunar surface, the objects fail by a considerable margin to account for the observed backscattering magnitude. To be conservative, we have chosen a value of k considerably larger (≈6 db) than *Hagfors*'s [1967]. *Hagfors*'s value would lead, of course, to an even larger discrepancy if used here. Using the value $\epsilon_r = 13$ deduced by *Burns* [1969] for the subregolith leads only to a 1 db increase in σ over that for $\epsilon_r = 9$.

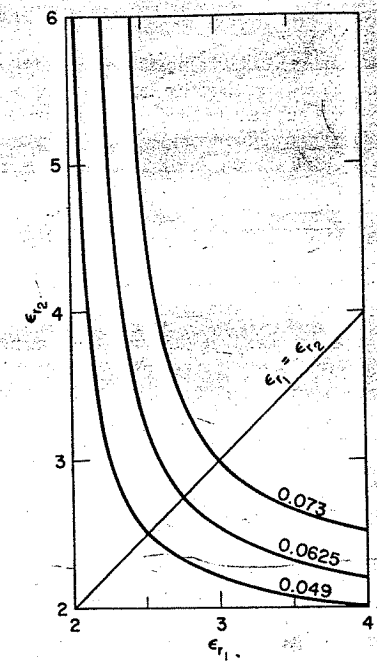

Fig. 11. Curves showing the relationship between the relative permittivities of the regolith (ϵ_{r_1}) and the bare rock surfaces (ϵ_{r_2}) for constant values of total quasi-specular cross section.

If we extrapolate the measured cross section per unit area from very high incidence angles such as $\cos\theta$, we obtain the values −19, −22, and −23 db at $\lambda = 3.8$, 23, and 68 cm, respectively. Scattering from the surface objects may be adequate to account for an important amount of this power. Thus the observed behavior at

high incidence angles may in some part be due to these objects.

In some localized areas, particularly the younger ones and the large recent craters, there may be a sufficient number of surface rocks to dominate the diffuse component. For instance, two atypical strewn fields at the Surveyor 3 landing site contain an order of magnitude greater number of the larger fragments [*Shoemaker et al.*, 1968], leading to a 10 db enhancement.

Appendix 2

Let us suppose that the cumulative number of objects of size $\geq y$ per unit volume in the regolith is given by $N(y) = N_0 y^{-m}$. Such distributions are commonly encountered in impact communition processes and are followed by the visible lunar surface objects [*Hapke*, 1968; *Meloy and O'Keefe*, 1968; *Shoemaker et al.*, 1968]. The number of objects per unit volume of size between y and $y + dy$ is $N(y)dy = mN_0 y^{-m-1}dy$.

Assume (as in Appendix 1) that each object presents a backscattering cross section equal to $(\pi/4)ky^2$ if y exceeds the wavelength and is zero otherwise [*Hagfors*, 1967]. Multiple scattering will be ignored since the reflectivities of the objects and the surface are small, and wavelength-size objects are expected to be relatively scarce. k is a factor involving the reflectivity of the individual objects. Except for the occasional large objects, the regolith will be assumed to be a homogeneous medium with relative permittivity ϵ_r and optical depth $a = l\lambda$, proportional to the wavelength. The objects will be taken to be uniformly distributed and to have no preferred orientation. Since the regolith is an attenuating medium, the contribution of each object to the cross section is $(\pi k y^2/4\epsilon_r)$ exp $(-2x/l\lambda)$ multiplied by the transmissivity product, where x is distance along the incident wave vector below the surface.

The cross section per unit area will then be

$$\sigma = \int_{\lambda}^{y_{max}} \int_{0}^{D} \frac{\pi mk}{4\epsilon_r} N_0 y^{-m+1} \cdot \exp(-2x/l\lambda)\, dx\, dy$$

if we do not include the transmissivity product. Assuming that the regolith is at least several optical depths thick, we let $D \to \infty$ and with $y_{max} \to \infty$ obtain

$$\sigma \cong \frac{\pi mkN_0 l}{8(m-2)\epsilon_r} \lambda^{3-m}$$

Clearly, the condition for wavelength independence is $m = 3$, corresponding to *Hapke's* [1968] 'critical spectral index,' and is the expected exponent of *Shoemaker et al.* [1968]. With $m = 3$,

$$\sigma = \frac{3\pi kN_0 l}{8\epsilon_r}$$

Let us now see if this mechanism can account for the magnitude of the observed backscattered power. The best way to do this seems to be to compute the required N_0. Suppose that $\epsilon_r = 3$ and $l = 17$ ($a \approx 10$ free-space wavelengths) and that the objects have a k appropriate for large spheres with $\epsilon_r = 9$. Then, $k = 0.07$ and $\sigma = 0.47\ N_0$. At normal incidence, σ should be reduced by 0.6 db to account for the transmissivity product. The observed value of σ extrapolated to normal incidence is about -17 db at 68 cm (Appendix 1). The corresponding N_0 is 0.049, hence the required distribution function is

$$N(y) = 4.9 \cdot 10^{-2} y^{-3}$$

where y is in meters and $N(y)$ is per cubic meter.

It is not clear how to compare this distribution with the observed visible object distributions from the Surveyor television observations since those are not volumetric distributions. Instead, let us suppose that the regolith has an overall porosity of 0.35 [*Jaffe*, 1968]. Then, taking the volume of each particle to be $(\pi/6)y^3$, the volume occupied by particles between y_{min} and y_{max}, assuming that the distribution law applies over the entire size range with $m = 3$, is

$$v = \frac{\pi}{2} N_0 \left[\ln \frac{y_{max}}{y_{min}}\right]$$

per unit volume. Setting $v = 0.65$, $y_{max} = 30$ meters, and $y_{min} = 0.3$ μm, we find $N_0 = 2.3 \cdot 10^{-2}$, in fairly good agreement with the radar derived value. Thus it appears that this model is able to account for the observed cross section.

Appendix 3

In Appendix 2, the regolith was assumed to be very deep compared to the optical depth. If there is no appreciable contribution to the backscatter from the subregolithic surface, and if the object distribution is independent of depth, the variation of cross section with regolithic depth will be that of Figure 12. Actually, Figure 12 is rather unrealistic where the regolithic depth approaches the wavelength because larger than wavelength-sized objects would not be buried. The 'volume cross section' would then decrease more rapidly than in Figure 12, but the 'surface cross section' would eventually dominate. Indeed, where the regolith is very thin there may be a larger number of surface fragments than rest on thicker regolith [*Oberbeck and Quaide*, 1968], possibly leading to an overall echo enhancement like that of large fresh craters.

The mean depth of the regolith has been estimated as varying between 3.3 and 16 meters in mare areas, with most of the estimates being about 4.6 meters [*Oberbeck and Quaide*, 1968]. The regolith is thought to be much deeper in the older highland regions [*Oberbeck and Quaide*, 1967]. It is worth noting that the part of the moon responsible for most of the high incidence angle backscattering happens to be primarily highlands and presumably has little or no reduction in cross section even at the longest wavelengths. In the mare, however, one would expect considerable reduction.

Indeed, *Thompson and Dyce* [1966] reported that 68-cm echoes from the mare were 1.5 to 2 times weaker than from the highlands. These values are in very good agreement with those predicted from Figure 12 for depths centered on 4.5 meters and for optical depths of 10 to 20 (free-space) wavelengths.

The above applies over very large areas. One may speculate, however, about the possibility of detecting changes over smaller areas, assuming that the buried scatterers model is correct. *Thompson's* [1968] 70-cm range Doppler maps should be ideal, from Figure 12 and the expected mare regolith depths, for observing intra-mare thickness changes. Since the older parts of a mare apparently have a deeper regolith [*Oberbeck and Quaide*, 1968], a comparison between the USGS geologic maps of the moon and the depolarized radar results should reveal many agreements. Although the correspondence is not exact, many mare areas which are thought to be younger do appear darker on the radar maps. In one instance, in the mare areas of the Sinus Iridum quadrangle [*Schaber*, 1966], the overall agreement is particularly striking. Also, the youngest mare areas do not appear to be the weakest diffuse reflectors in general. It is hoped that a fuller report on this subject can be made in the near future.

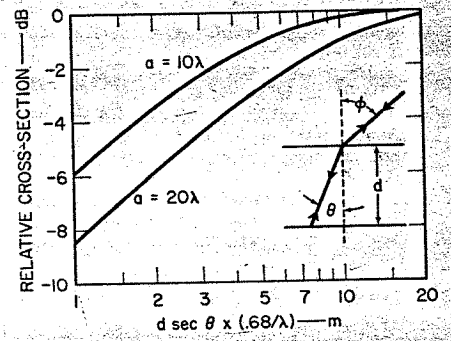

Fig. 12. Reduction in cross section due to scattering volume limitations, normalized to $\lambda = 68$ cm. d = depth of regolith and a = optical depth in regolith.

Thus the 70-cm radar maps may be a very useful tool in determining the relative age of mare areas. Since the highland areas are apparently must deeper, a greater wavelength would be needed to 'plumb' them. This theory predicts that there should be little difference seen between the depolarized echoes from mare and highlands at very short wavelengths. The results of the 3.8-cm mapping currently being undertaken at Lincoln Laboratory may well be a good test of the theory.

Acknowledgments. I would sincerely like to thank Dr. G. L. Tyler for his many contributions. The assistance of Mrs. Dolores McNiel is greatly appreciated. Many illuminating discussions with Dr. C. A. Lofgren should also be acknowledged.

References

Beckmann, P., Radar backscatter from the surface of the moon, *J. Geophys. Res.*, *70*(10), 2345–2350, 1965.

Beckmann, P., Depolarization of electromagnetic waves backscattered from the lunar surface, *J. Geophys. Res.*, *73*(2), 649–656, 1968.

Born, Max, and Emil Wolf, *Principles of Optics*, Pergamon Press, Oxford, 1965.
Burns, Alan A., On the wavelength dependence of radar echoes from the moon, accepted for publication, *J. Geophys. Res.*, 1970.
Evans, J. V., and T. Hagfors, Study of radio echoes from the moon at 23 centimeters wavelength, *J. Geophys. Res.*, *71*(20), 4871–4889, 1966.
Evans, J. V., and G. H. Pettengill, The scattering behavior of the moon at wavelengths of 3.6, 68 and 784 centimeters, *J. Geophys. Res.*, *68*(2), 423–447, 1963.
Hagfors, T. A study of the depolarization of lunar radar echoes, *Radio Science*, *2*(5) (New Series) 445–465, 1967.
Hagfors, T., and J. Morriello, The effect of roughness on the polarization of thermal emission from a surface, *Radio Sci. J. Res. NBS, 69D*, 1614–1615, 1965.
Hapke, B. W., On the particle size distribution of lunar soil, *Planet. Space Sci.*, *16*(1), 101–110, 1968.
Heiles, C. E., and F. D. Drake, The polarization and intensity of thermal radiation from a planetary surface, *Icarus*, *2*, 281–292, 1963.
Jaffe, L. D., et al., Principal scientific results of the Surveyor 3 mission, *J. Geophys. Res.*, *73*(12), 3933–3987, 1968.
Jones, B. P., Density-depth model for the lunar outermost layer, *J. Geophys. Res.*, *73*(24), 7631–7635, 1968.
Lincoln Laboratory, *Radar Studies of the Moon, Final Report*, vol. 1, (contract NSR 22-009-106), Feb. 15, 1967.
Lincoln Laboratory, *Radar Studies of the Moon, Quarterly Progress Report No. 4*, (contract NSR 22-009-106), Nov. 15, 1966.
Meloy, T., and J. A. O'Keefe, Size distribution of lunar surface materials, *J. Geophys. Res.*, *73*(6), 2299–2301, 1968.
Morris, E. C., et al., Television observations from Surveyor 6, in *Surveyor 6, A Preliminary Report*, NASA SP-166, March 1968.
Muhleman, D. O., Radar scattering from Venus and the moon, *Astron. J.*, *69*, 34–41, 1964.
Oberbeck, V. R., and W. L. Quaide, Estimated thickness of a fragmented surface layer of Oceanus Procellarum, *J. Geophys. Res.*, *72*(18), 4697–4704, 1967.
Oberbeck, V. R., and W. L. Quaide, Genetic implications of lunar regolith thickness variations, *Icarus 9*(3), 446–465, 1968.
Rea, D. G., N. Hetherington, and R. Mifflin, The analysis of radar echoes from the moon, *J. Geophys. Res.*, *69*(24), 5217–5223, 1964.
Schaber, G. G., *Preliminary Geologic Map of the Sinus Iridum Quadrangle of the Moon*, Department of the Interior, United States Geological Survey, 1966.
Shoemaker, E. M., et al., Television observations from Surveyor 5, in *Surveyor 5, A Preliminary Report*, NASA SP-163, Dec. 1967.
Shoemaker, E. M., et al., Television observations from Surveyor 3, *J. Geophys. Res.*, *73*(12), 3989–4044, 1968.
Smith, Bruce G., Boulder distribution analysis of the Luna 9 photographs, *J. Geophys. Res.*, *72*(4), 1398–1399, 1967.
Thompson, T. W., and R. B. Dyce, Mapping of lunar radar reflectivity at 70 cm, *J. Geophys. Res.*, *71*(20), 4843–4853, 1966.
Thompson, T. W., Radar studies of the lunar surface emphasizing factors related to selection of landing sites, *Research Report RS73, Final Report, Center for Radiophysics and Space Research, Cornell University*, Ithaca, New York, April 1968.
Tyler, G. L., Oblique-scattering radar reflectivity of the lunar surface: Preliminary results from Explorer 35, *J. Geophys. Res.*, *73*(24), 7609–7620, 1968.

(Received April 23, 1969;
revised July 24, 1969.)

Paleomagnetism of Franciscan Ultramafic Rocks from Red Mountain, California

AFIF HANI SAAD[1]

Department of Geophysics, Stanford University, Stanford, California 94305

Results from the study of the magnetism in serpentinized ultramafic rocks of the Red Mountain intrusion southeast of San Francisco, California, suggest that these rocks possess a chemical remanent magnetization acquired during serpentinization. The stability of magnetization decreases with serpentinization, owing to the growth of larger magnetic grains. Thus, in highly serpentinized peridotites (serpentinites), most of the CRM is destroyed and the NRM becomes mainly viscous remanent magnetization, rendering these rocks unsuitable for paleomagnetic work. On the other hand, in partially serpentinized peridotites, pyroxenites, and dunites, the CRM is highly stable and paleomagnetically reliable. A study of the stable directions of magnetization indicates that the Red Mountain ultramafic body was emplaced and serpentinized prior to the folding of the Franciscan formation. The stability of magnetization and removal of viscous components were verified by the results of a storage test and alternating-field demagnetization experiments, by the divergence of the mean directions of magnetization from that of the present field, and, most important, by the convergence of the directions after tilt correction. Paleomagnetic pole positions calculated from the mean directions suggest that the magnetic pole rapidly migrated southward into the Atlantic Ocean during late Mesozoic, possibly more than once, as proposed previously by Grommé and Gluskoter.

INTRODUCTION

A study of ultramafic rocks covering different degrees of serpentinization was conducted for the purpose of investigating their magnetic properties. Samples were collected from Red Mountain, Mount Boardman Quadrangle, California, a large ultramafic body intruding the uppermost part of the exposed Franciscan section in the Diablo Range (Figure 1). The investigation consisted of two parts: (1) a study of intensity of induced and remanent magnetism, and (2) a study of directions of remanent magnetism.

Results of the first study, described in another paper [*Saad*, 1969], indicated that the susceptibility and intensity of remanent magnetism are highly variable, depending largely on the degree of serpentinization and, to a lesser extent, on the original rock composition. The remanent magnetization in these ultramafic rocks was found to be mainly a chemical remanent magnetization (CRM) acquired during the process of serpentinization whereby iron atoms, released from the silicate structure of the paramagnetic olivine and pyroxene, are oxidized to form ferrimagnetic magnetite. As serpentinization increases, the natural remanent magnetization increases in intensity but decreases in stability because of the growth of magnetite grains from single- to multi-domain size and of their oxidation, in some cases, to maghemite.

This paper deals with the paleomagnetic reliability and significance of the directions. The main objectives of the study were (1) to investigate more thoroughly the stability of the natural remanent magnetization (NRM) observed in these rocks and to confirm its origin, (2) to test whether ultramafic rocks can be used reliably for paleomagnetic work, and (3) to find the paleomagnetic pole position and examine its compatibility with previously reported poles from North America. The paleomagnetic data in this paper are analyzed in connection with the general problem of easterly directions found first by *Cox* [1957] and later by *Grommé and Gluskoter* [1965] from late Mesozoic and early Tertiary rocks of the western United States. The problem is of some interest since these

[1] Now at the Department of Geology, University of Missouri, Rolla, Missouri 65401.